Lab on a Chip

Accepted Manuscript

ROYAL SOCIETY OF CHEMISTRY

www.rsc.org/loc

Lab on a Chip

RSCPublishing

ARTICLE

A Microfluidic Linear Node Array for the Study of Protein-Ligand Interaction

Cite this: DOI: 10.1039/xoxxoooooox

Cheuk-Wing Li[a]*, Guodong Yu[a], Jingyun Jiang[a], Simon Ming-Yuen Lee[a], Changqing Yi[b], Wanqing Yue[c], Mengsu Yang[c]

Received ooth January 2012,
Accepted ooth January 2012

DOI: 10.1039/xoxxoooooox

www.rsc.org/

We have developed a microfluidic device for continuous separation of small molecules from a protein mixture and demonstrated its practical use in the study of protein-ligand binding, a crucial aspect in drug discovery. Our results demonstrated dose-dependent binding between bovine serum albumin (BSA) and its small-molecule site marker, Eosin Y (EY) and the binding reached plateau when BSA:EY ratio was above 1, which agreed the eosin binding capacity of BSA reported in literature. By streamline control using a combination of two fundamental building blocks (R, L nodes) with microdevice operated at a high flow rate (up to 1300μL h^{-1}), a solution barrier was created to "filter" off protein/protein-ligand complexes such that the small unbound molecules were isolated and quantified easily. The percentage decrease of small molecules with increasing protein concentration indicated the presence of binding events. Several fluorophores with different molecular weight were used to test the performance of the microfluidic "filter", which was tunable by 1) total flow rate and/or 2) flow distribution ratio between the two device inlets; both were easily attainable by changing syringe pump settings. Since the microdevice was operated at a relatively high flow rate, aliquots were easily recovered from the device outlets to facilitate off-chip detection. This microfluidic design is a novel and promising tool for preliminary drug screening.

1. Introduction

Many unique functions in microfluidic devices are achieved by controlling the movement of fluid streams within microchannels. To name a few, streamline control aids in treatment of cells by stepwise exchange of solution[1], enhances the capture of circulating tumor cells by promoting the contact between fluid streams and the surface of microchannel immobilized with antibodies[2, 3], assists the arraying of functionalized microspheres for DNA and protein analysis[4, 5], enables the separation of particles and blood cells by deterministic flow engineered in an array of pillar structures[6]. While each microfluidic design can be engineered as a whole to serve a particular purpose, it could be a more efficient design strategy to achieve different unique purposes by creating and scripting certain fundamental building blocks with predictable fluidic behavior. Recently, using pillar structure as a fundamental unit, together with using fast flow speed, splitting of fluid streams, solution exchange and particle separation has been demonstrated in a programmable fashion[7]. It has also been shown that by using fundamental nodes R, L , Z and N, the fate of streamlines are programmable in a 2D array, though no practical application has been demonstrated[8]. In this study, we have employed the fundamental R, L nodes in a linear array to achieve separation of small molecules from a protein mixture. The design is capable to work at fast flow rate to serve for preparative purposes.

R and L nodes are tangential microchannels originally designed for flow switching. It is a crossing microstructure formed by a stack of two straight channels, where each channel is featured on an individual layer of PDMS and the 2 layers are then face-to-face bonded[9]. Tangential microchannels have been employed in several two-layer micromixers where chaotic mixing is provoked to evenly distribute sample and buffer streamlines across the device outlet[10-12]. Rather than enhancing chaos for complete mixing, our linear node array systematically opened up buffer streamlines, interlacing the buffer and sample streamlines to shorten the diffusion distance, followed by retrieval of buffer streamlines carrying with a certain amount of diffused species. As a result, a diffusion-biased recovery of small molecules from a protein mixture was demonstrated in a continuous fashion when the device was operated at a volumetric flow rate up to 1300μL h^{-1}, which also facilitated off-chip sample analysis of processed solution.

Furthermore, we have applied the continuous separation function in the study of protein-ligand interaction, which is crucial for almost all biological functions and designing safe therapeutics[13]. This simple protein-ligand interaction model consisted of BSA, the most abundant blood plasma protein which binds with certain drugs and alters their effective dosage [14] and EY, a site I marker of BSA[15] with BSA:EY binding ratio = 1 at physiological pH and room temperature[16]. Currently, equilibrium dialysis is the gold standard for plasma protein binding but normally a 12-hour incubation time is required for complete equilibration of small ligand across a physical barrier,

i.e., a filter membrane with fixed molecular cut-off size[17]. In contrast, our continuous separation design required no physical barrier so that protein-ligand binding event was successfully monitored within several minutes. We leveraged the fluidic behavior in microchip to achieve filtering function so that different molecular cut-off sizes were easily attainable by different syringe pump settings.

2. Materials and methods

2.1 Reagents.

~5500μL^{-1} of 2 μm fluorescent microspheres were resuspended in Mili-Q water with 1% TWEEN® 20, 50 μM of DexRhoB (Rhodamine B isothiocyanate–Dextran, average mol wt ~10,000), 1.3 μM of AlbuFITC (Albumin–fluorescein isothiocyanate conjugate), 20 μM of Eosin Y (EY) and bovine serum albumin (BSA) were purchased from Sigma (St. Louis, MO, USA). 2 μM of R110 (Rhodamine 110) was purchased from Molecular Probes Inc (Eugene, OR, USA). All species used in on-chip analysis were dissolved in Hank's balanced salt solution (Gibco, Carlsbad, CA, USA) added with a working concentration of 0.1% DDM (n-Dodecyl β-D-maltoside, Sigma) to minimize non-specific protein absorption in microchip[18].

2.2 Microchip fabrication.

The linear node array was prepared by molding polydimethylsiloxane (PDMS) against a printed circuit board (PCB) master with detail described elsewhere[19-21]. In brief, the procedure involved transferring photomask patterns on the photoresist of the PCB (Kinsten, Chiefskill, Taiwan) by UV irradiation followed by the removal of exposed photoresist, the etching of the unprotected copper layer and the casting of PDMS (RTV 615, GE Silicones, Waterford, NY, USA) on the PCB master. Negative replicas bearing channel feature (20 x 100μm; H x W) were peeled off from the master and sealed by a dipping-attaching method [22, 23] after circular holes were punched through the top layer.

2.3 Instrumentation and data analysis.

For on-chip interrogation of dye species, mixtures (Mixture 1: AlbuFITC + DexRhoB, Mixture 2: R110 + DexRhoB) and buffer solution were injected into the linear node array using two positive displacement syringe pumps (KDS270P, KD Scientific, USA) while the waste and recovery outlets were left opened to the atmosphere. Micrographs were taken from an inverted fluorescence microscope (IX73, Olympus, Japan) equipped with a cooled CCD camera (DP72, Olympus, Japan) using 4x and 20x objectives. A fluorescence light source (X-Cite Series 120Q, Olympus, Japan) with filter set BP460-500, BP505-555 was used for R110, AlbuFITC and EY while filter set BP510-560, BP 583-658 was used for DexRhoB.

The mixture and buffer solution were injected into the microdevice by the volumetric flow rates as tabulated in Table 1 to reach different flow distribution ratios (FD). Each FD configuration was continuously monitored to retrieve stabilized data (at least 120 seconds). Background and dye flooded images were retrieved by 120 seconds of washing with buffer solution, followed by another 120 seconds of filling the entire node array with dye species at the same total flow rate for a particular FD configuration (either 325μL h^{-1} or 1300μL h^{-1}). Background-corrected and normalized fluorescence intensity profiles were retrieved by ImageJ and the area integral of pure dye species at the recovery channel was analyzed in Excel for the calculation of percentage recovery: **%rec**. A 4x objective was used to capture the entire node array for bead trajectories.

	Total 325μL h^{-1} **(Re ~ 1)**		**Total** 1300μL h^{-1} **(Re ~ 4)**	
Target Inlet-FD	**Mixture (μL h^{-1})**	**Buffer (μL h^{-1})**	**Mixture (μL h^{-1})**	**Buffer (μL h^{-1})**
0.1	30	295	118	1182
0.2	54	271	217	1083
0.4	93	232	371	929
0.6	122	203	488	813
1	163	163	650	650
2	217	108	867	433
4	260	65	1040	260
10	295	30	1182	118

Table 1. Volumetric flow rate applied in mixture and buffer inlets to achieve the targeted flow distribution ratio (i.e. inlet-FD). The flow rates are rounded off to the nearest whole number to match the targeted FD.

In off-chip preparative mode, FD-0.6 configuration was used to inject a mixture of EY and BSA with buffer solution into microdevices that were placed within homemade humidity chambers to minimize evaporation. After 20 minutes washing, solution was collected from both outlets at 15-min intervals and added with 3 folds of buffer solution for matrix matching. All samples and calibration solutions were pipetted into 384-well plates and results were taken from an automated imaging system (IN CELL Analyzer 2000, GE Healthcare, UK; DAPI excitation filter and Cy3 emission filter) to determine the concentration of EY. Calibration curves with R^2 up to 0.999 were obtained from pure EY at different concentrations. The percentage recovery by off-chip detection, $\%rec_{off}$, was calculated by dividing the EY concentration of solution collected from the recovery outlet against the known concentration of EY injected into the microfluidic chip.

In each section and every flow configuration, at least replicated experiments were performed on individual replicas such that the error bars reflected the impact of misalignment among replicas.

2.4 Simulation model.

The velocity field and pressure profiles in the linear node array was simulated by a commercial computational fluid dynamics package (FLUENT 6.2, Fluent Inc, Lebanon, NH) with meshes constructed by GAMBIT (FLUENT, Inc)[24]. The 3D model was composed of grid patterns with ~1,000,000 nodes. Microchannel cross section was simplified as regular rectangle with 100 μm in width and 20 μm in height, which were comparable to the actual device. Two Newtonian fluids of identical densities and viscosities were simulated as inlet solution. The standard Navier-Stokes equation with velocity-inlet and pressure-outlet boundary conditions was solved to determine the streamlines. Fluidic flows were assumed as steady-state laminar flows and no slip condition was imposed at all the boundaries. Eighty streamlines across each inlet were tracked using simulated particle injections[25]. Convergence criterions of residual monitor for all quantities (continuity, x-, y-, z-flow velocity) were set to 10^{-5}.

3. Results and discussion

3.1 Design principle

Our discussion begins by considering streamline control in two prominent designs that are widely used in microfluidic systems, i.e., the chaotic mixer[26] and the T sensor[27]. For a chaotic mixer having two inlets and outlets, the streamlines originated from any inlets will be evenly distributed among both outlets. On the other hand, streamlines originated from an inlet of the H filter (i.e. a T sensor with two outlets) are recovered at the outlet of the same side with respect to that inlet. Our linear node array is designed to control streamlines in a way that resembles a hybrid of the chaotic mixer (enhanced solute mixing) and the H filter (no mixing of streamlines). Purposed for a diffusion-biased recovery of small molecules, the node array enhances interfacial contact among streamlines originated from sample and buffer inlets, but buffer streamlines will only be retrieved at buffer outlet and vice versa for sample streamlines, rather than evenly distributed between both outlets.

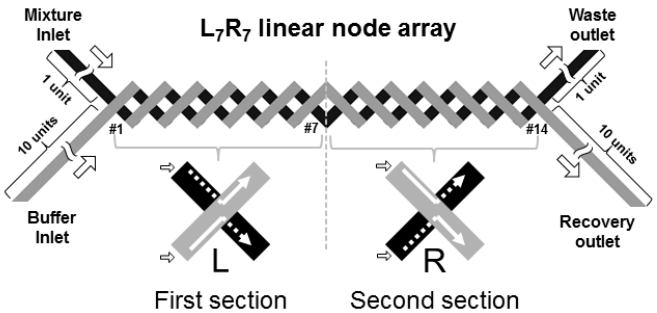

Fig 1 schematic diagram of the design: The linear node array is comprised by a stack of straight channels featured on bottom (black) and top (gray) layers of PDMS substrate that are face-to-face bonded. L and R nodes are named by the way of streamline steering: left-handed and right-handed alpha helix, respectively. Inlet-FD-10 is determined by the length of the buffer microchannel that is 10 times longer than the mixture microchannel. Likewise, outlet-FD-10 is determined by the length of recovery channel that is 10 times longer than the waste channel. The direction of fluid flow is depicted by white arrows, nodes are numbered from left to right, and there is a gray dotted line between node #7 and #8, showing the mirror architectural design of this linear node array.

Based on our previous nomenclature system[8], the linear node array used in this study is referred to as $\mathbf{L_7R_7}$ (Fig 1) and it is comprised of two layers of straight channels that are face-to-face bonded. Splitting and recombination of fluidic streamlines are expected to take place among all stacking positions of the microchannels. With a channel aspect ratio of 20/100 (height/width), the first section of seven L nodes triggers a cycle of the lamination process while the second section of seven R nodes reverses such lamination by a mirror image architecture as shown in the simulation result (Fig 2, dotted line depicted the mirror plane). Streamlines in the $\mathbf{L_7R_7}$ was revealed experimentally using 2μm microspheres (Fig 3a and b).

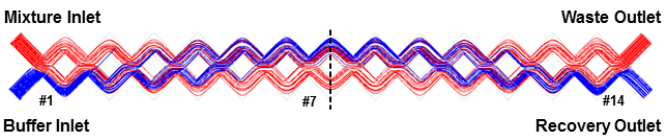

Fig 2 Computation simulation of streamline trajectories in $\mathbf{L_7R_7}$, where a majority of streamlines from the buffer inlet (blue) were traversed to the upper side after the #7 L node. These buffer streamlines were rendezvous at the recovery outlet after the #14 node. Interlacing of mixture and buffer streamlines were observed between nodes #2 and #13.

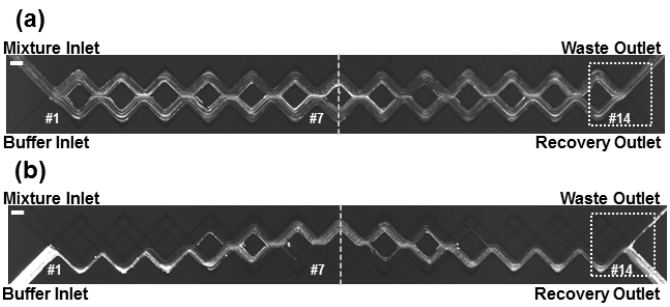

Fig 3 Particle trajectories and streamline recollection at default flow distribution, FD-10: 2 μm polystyrene microspheres were introduced from a) mixture inlet and b) buffer inlet. There was a characteristic stream of particles leaked towards the waste outlet in b) and it was attributed to bifurcation law that is only applicable to particle entities. Scale bar on the top left corner is 100μm.

Large and small molecules are expected to have different fate when passing through this channel architecture. For example, when two syringe pumps displace a total flow rate of 1300μL h^{-1}, the average residence time of the $\mathbf{L_7R_7}$ is about 0.04 seconds and the mean diffusion distance for AlbuFITC and R110 are 0.3μm[28] and 0.8μm[29], respectively. Assuming the shortest distance between buffer and mixture streamline is 0.4μm, R110 molecules can easily travel from mixture to buffer streamlines while only a smaller-than-average amount of AlbuFITC molecules can manage to reach buffer streamlines within the average residence time. In this way, buffer streamlines will preferentially carry more R110 than AlbuFITC molecules when they rendezvous at the recovery outlet, just as the mixture streamlines will convectively transport towards the waste outlet as shown in Fig 3a.

The **recovery ratio** (i.e. **%rec** of small /large molecules at the recovery outlet) can be fine-tuned with different flow distribution ratios (FD) that is easily attainable by pumping different volumes of solution through the two inlets. By design, both the inlet-FD (flow rate of mixture/buffer inlets) and the outlet-FD (flow rate of waste/recovery outlets) of this node array are set to 10. The inlet and outlet-FD are determined by the 10: 1 length ratio between inlet and outlet channels connecting the access vials and the node array (Fig 1). The default inlet-FD-10 can be overridden by syringe pumps displacing constant flow volume. Since Newtonian fluid is incompressible, any inlet-FD smaller than 10 indicates a decreased amount of mixture streamlines entering the node array. With lesser amount of both small and large species but preferred recovery of small species, a higher **recovery ratio** could be achieved by reducing inlet-FD so that only negligible amount of large species could manage to reach the recovery outlet. For the same purpose, by applying a higher total flow rate, it will be more difficult for both small and large species to travel across streamlines but small molecules will be preferential recovery because they can get across streamlines more effectively.

Therefore, by tuning the FD configuration and the total flow rate, the linear node array can create a cut-off window to minimize the recovery of large molecules. It is also worth noting that the mirror architectural design in $\mathbf{L_7R_7}$ since high flow speed was employed in our study. Channel deformation

was observed (inflation) due to the inherent elasticity of PDMS substrate under high flow pressure. Such deformation in effect altered our engineered channel aspect ratio that could ultimately deteriorate the performance of streamline recollection. The deformation issue was cancelled out by using the mirror architecture where identical amount of R nodes were arranged to deform together with the L nodes. Throughout this study, the linear node array performed as expected in a wide range of total flow rates starting from 110 to 1300μL h^{-1}.

3.2 Streamline trajectories in L_7R_7 linear node array.

Since micron sized particles are insensitive to diffusion, 2μm fluorescent beads (~ 0.22 $\mu m^2 s^{-1}$ estimated by Stokes-Einstein equation[30]) were employed to study the streamline trajectories in the linear node array. At the default Inlet-FD-10 configuration (Table 1), we have separately introduced fluorescent beads from mixture (Fig 3a) and buffer (Fig 3b) inlets. To visualize the spatial distribution of streamlines, we recorded fluorescence images of the node array in long exposure time so that individual beads were exhibited as trajectories. Furthermore, quantitative measurement of particle recovery was implemented by taking movies at the node #14 position with 20x objective so that individual beads were able to be counted manually (supplementary data S1).

Fig 3a illustrated the representative streamline trajectories of the node array at default FD-10 when beads were introduced from the mixture inlet and exited at the waste outlet, with a streamline recollection of 97.7% ± 1.5%. Beads introduced from the buffer inlet were expected to be retrieved at the recovery outlet (Fig 3b), however, the streamline recollection was only 92.7% ± 2.6%, with a characteristic streamline "leaked" towards the waste outlet. In addition to imperfections in microfabrication and layer alignment processes, we believe the bifurcation law[31] (that only applicable to particle entities) should have played a major role to the loss of microspheres at node #14, where the flow rate in the waste outlet was 10 times higher than that in the recovery outlet. After all, more than 90% of buffer streamlines reached their target destination, the recovery outlet.

From the streamline trajectories we observed mixing and unmixing phenomenon within the $\mathbf{L_7R_7}$ linear node array: In Fig 3b, the originally pitched buffer streams (after node #1) were spread across the entire microchannel of 100μm in width (after node #7) and retrieved at recovery outlet (after node #14). Taking metro system as an analogy, this microdevice offers two railway lines (Line 1: mixture to waste, Line 2: buffer to recovery) and all passengers (diffusing species) are originally taking the Line 1. Splitting and recombination of solution increased the points for cross-platform interchange between Line 1 and Line 2. If a passenger (fast diffusing species) manages to travel a short distance across the platform and catches a train on Line 2, one will arrive at a destination (to recovery outlet) different from the rest who stays on Line 1(to waste outlet).

3.3 On-chip separation of small molecules by L_7R_7 linear node array.

After streamline recovery was verified, we further tested the linear array with different inlet-FD (i.e. flow rate of mixture/buffer inlets) to optimize the separation of small molecules. The FD settings used in this experiment were listed in Table 1. Notice that the syringe pumps could only override the inlet-FD while outlet-FD-10 was fixed. By varying inlet-FD configuration from 0.1 to 10, the **%rec** of different dye species (diffusion coefficient of R110[32], 10kDa DexRhoB[33] and AlbuFITC[28] are 430 $\mu m^2 s^{-1}$, 130 $\mu m^2 s^{-1}$ and 61 $\mu m^2 s^{-1}$ respectively) at the recovery outlet were shown at different total flow rates, 325μL h^{-1} in Fig 4a and 1300μL h^{-1} in Fig 4d. Since the majority amount of both species were delivered by the mixture streamlines at high flow speed, negligible extent of diffusion-biased recovery was observed at the waste outlet.

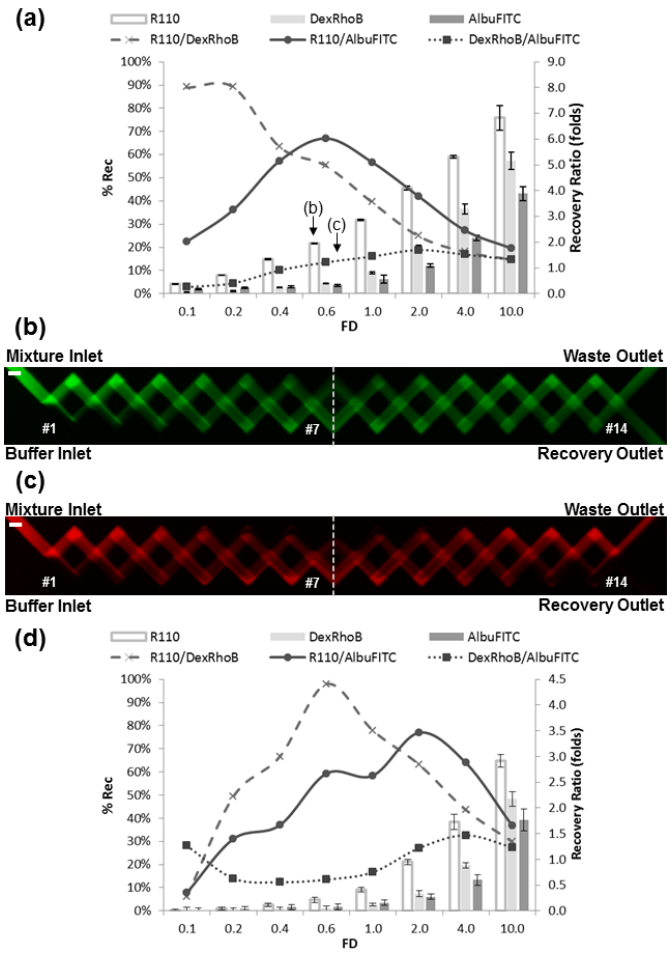

Fig 4 a) Diffusion-biased recovery of small molecules at various FD configurations from 0.1-10: The columns of the chart represents the **%rec** of the three species (the left y-axis) while the lines represents the **recovery ratio** between two species under a particular FD (the right y-axis). Molecular weight for R110 (small), DexRhoB (medium) and AlbuFITC (large) species are 366.8Da, ~ 10kDa and ~ 67kDa respectively. Optimized FD for R110 recovery against protein was FD-0.6 at a total flow rate of 325μL h^{-1}. Pseudo-color images showing the spatial distribution of R110 b) and AlbuFITC c) within the linear node array operated at FD-0.6, 325μL h^{-1}. Scale bar on the top left corner is 100μm. d) Optimized FD for R110 recovery against AlbuFITC was shifted to FD-2 at a total flow rate of 1300μL h^{-1}.

Starting from the default inlet-FD-10, where streamline trajectories was resemblance to Fig 3b, buffer streamlines were spread to contact with 10 times the amount of mixture streamlines carrying dye species. Fig 4a suggested that even the slowest diffusing AlbuFITC managed to have over 40% recovery in this configuration. To create a more stringent cut-off window for larger molecules, either reducing FD or increasing total flow rate could be performed. Reducing FD

decreased the relative amount of mixture streamlines getting into the node array such that the recovery of larger species could be suppressed. From the curve of R110/AlbuFITC in Fig 4a, **recovery ratio** was maximized at FD-0.6 configuration, in which 21.7±0.2% of R110, 4.4±0.3% of DexRhoB and 3.6±0.4% of AlbuFITC were recovered. Pseudo-colored dye pattern of R110 and AlbuFITC captured at identical FD and total flow rate were shown in Fig 4b and Fig 4c. From these fluorescence micrographs, an observable amount of R110 species was retrieved at the recovery outlet while the recovery of AlbuFITC was barely noticeable. Likewise, the **recovery ratio** was maximized when FD-0.2 was used for the separation of R110 and DexRhoB.

Since a cut-off window for large molecules can be also achieved by using a higher volumetric flow rate, we performed another set of experiments by increasing the total flow rate to 1300μL h^{-1} (the flow rate was chosen by the fact that even the fastest diffusing species, R110, was not recovered in FD-0.1 configuration). As shown in Fig 4d, the optimal recovery between R110 and AlbuFITC shifted toward a higher FD-2 and the **recovery ratio** was decreased to ~3.5 folds, albeit the total flow rate was increased by 4 times, which increased the solution throughput of the microdevice. We have employed the flow rate of 325μL h^{-1} for the rest of our experiments because the incident of channel clogging by fiber/debris increased when using 1300μL h^{-1} for long-term separation ,i.e., >1 hour experiment in preparative mode.

3.4 Protein-small molecule binding study by L_7R_7 linear node array

Although it is ideal to handle all fluid manipulation and detection on the same chip, the benefits of off-detection is undeniable. For example, molecular absorption spectrometry can be used to study many drug compounds that are non-fluorescent. Non-specific absorption on PDMS that hinders on-chip quantitative analysis can be improved by off-chip detection. However, the flow rate used in many microfluidic systems is often too low for preparative purpose[34, 35]. To test the feasibility of protein-ligand binding and off-chip detection, we employed a model mixture consisted of BSA (one of the major components in plasma protein) together with its site marker, EY[36]. The binding site number for EY in BSA is ~1 at physiological pH and room temperature[16]. Protein-ligand binding was evaluated by using variable concentrations of BSA against a fixed concentration of EY at 20μM.

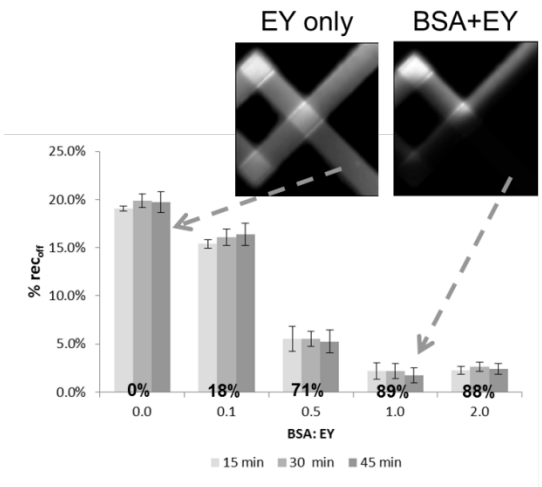

Fig 5 The study of protein-ligand binding by the microchip: Different ratio of BSA: EY mixtures were injected into the microchip and quantitative detection of EY concentration was determined off-chip by an automated imaging system. By comparing the inset images and their corresponding datum, a significant reduction of EY signal at the recovery outlet was observed when BSA: EY ratio was above 1. The bound % of EY on protein was calculated under each set of columns. The stability of off-chip **%rec$_{off}$** over time was also evaluated by collecting aliquots from both the waste and recovery outlets at 15-min intervals after the outlet vials were washed by buffer solution for 20 minutes. Results demonstrated the microchip generated stable solution output for 45 mins.

Each microdevice was secured in a homemade humidity chamber to minimize evaporation of solution retrieved at the outlets. The device was allowed to wash for 20 minutes using the buffer solution, and then FD-0.6 configuration was employed at a total flow rate of 325μL h^{-1} (the highest **recovery ratio** was achieved in accordance with Fig 4a). It is known that the binding of EY and BSA completes within several minutes and the complex is stable for at least 1 hour[37] so equilibrium concentrations should have been reached for BSA and EY during the washing step. Then, the device was allowed to run continuously for another 45 minutes and aliquots were retrieved from the waste and recovery outlets at 15 minutes intervals for off-chip detection. As shown in Fig 5, **%rec$_{off}$** values were stable over the entire course of experiment at different BSA: EY ratios. Inset of Fig 5 (labeled with "EY only") illustrated the micrograph of microchip at node #14 position where **%rec$_{off}$** of EY was 19.5±0.9% in the absence of BSA. When BSA was added in the mixture, EY signal decreased gradually and reached a plateau until the ratio between BSA and EY was above 1. It was because the small EY molecules were bound on their protein targets that were restricted from reaching the recovery outlet at FD-0.6 configuration by referring to Fig 4c (Note: AlbuFITC is BSA conjugated with FITC). Under each set of columns in Fig 5, the bound percentage of EY on BSA was calculated by:

$$Bound\ \% = \frac{(\%\boldsymbol{rec_{off}}\text{ in EY only}) - (\%\boldsymbol{rec_{off}}\text{ of BSA: EY})}{(\%\boldsymbol{rec_{off}}\text{ in EY only})}$$

The results demonstrated the feasibility of this linear node array to quantitatively measure the binding between protein and small molecules and the device was operated at a flow rate high enough for preparative purposes to enable off-chip detection.

Conclusions

We have developed a microfluidic linear node array that continuously separated small molecules from a protein mixture based on diffusion at a flow rate of 325μL h^{-1}. Scripting the fundamental building blocks of R and L nodes in $\mathbf{L_7R_7}$ enabled interlacing and subsequent recollection (over 90%) of streamlines. At a particular flow rate, FD between inlets could be tuned to generate a "filter" barrier that restricted larger protein molecules from entering the recovery outlet while smaller molecules were preferentially recovered. Under optimal conditions (FD-0.6 and 325μL h^{-1}), on-chip **%rec** for R110, DexRhoB and AlbuFITC were 21.7±0.2%, 4.4±0.3% and 3.6±0.4% respectively, with a **recovery ratio** of ~ 6 folds between R110 and AlbuFITC. Since the microdevice was operated at a relatively high flow rate, off-chip detection was performed with aliquots retrieved from device outlets and quantitative analysis of the binding between protein and small molecules was carried out. Our results demonstrated dose-dependent binding between BSA and EY that reached plateau

when BSA: EY ratio was above 1 and only 15 minutes was required to collect each data point for off-chip detection. While separation between small and large molecules can also be performed by batch process such as dialysis or chromatographic methods, our device offers an alternative approach that conduct separation in a continuous fashion. Moreover, instead of materially changing the filter membranes of different pore sizes in dialysis or stationary phase with different sieving sizes in chromatography, molecular cut off size can be tuned by using different inlet-FD and total flow rates that are easy attainable by changing the flow settings. The capability for continuous separation at high flow rates makes this microdevice an eligible choice for preparative purposes and opens up the possibility to study protein-ligand interaction efficiently.

Acknowledgements

C.-W. Li would like to thank Professor Richard N. Zare for his guidance during Li's postdoctoral study in Stanford University. The work was supported by grants from the University of Macau (MYRG108(Y1-L2)-ICMS13-LCW, MYRG2014-00179-ICMS-QRCM), the National Natural Science Foundation of China (51102097) and Guangzhou Science and Technology and Information Bureau (2013J2200053, 2014J4100108).

Notes and references

[a] *State Key Laboratory of Quality Research in Chinese Medicine, Institute of Chinese Medical Sciences, University of Macau, Macau SAR, China. E-mail: cheukwli@umac.mo; Tel.: + 853 83978513; fax: + 853 2884 1358;*

[b] *Key Laboratory of Sensing Technology and Biomedical Instruments (Guangdong Province), School of Engineering, Sun Yat-Sen University, Guangzhou, China.*

[c] *Key Laboratory of Biochip Technology, Biotech and Health Centre, Shenzhen Research Institutes of City University of Hong Kong, Shenzhen, China.*

† Electronic Supplementary Information (ESI) available: [S1: Movie clip showing the **%rec** of particles. A movie clip captured at the #14 node of the $\mathbf{L}_7\mathbf{R}_7$ when operated at Inlet-FD-10 and a total flow rate of 110μL h^{-1}. 2μm polystyrene microspheres were introduced at the mixture inlet. As expected, almost all microspheres were collected at the waste outlet.]. See DOI: 10.1039/b000000x/

References

1. M. Yamada, J. Kobayashi, M. Yamato, M. Seki and T. Okano, *Lab Chip*, 2008, 8, 772-778.
2. S. Nagrath, L. V. Sequist, S. Maheswaran, D. W. Bell, D. Irimia, L. Ulkus, M. R. Smith, E. L. Kwak, S. Digumarthy, A. Muzikansky, P. Ryan, U. J. Balis, R. G. Tompkins, D. A. Haber and M. Toner, *Nature*, 2007, 450, 1235-1239.
3. S. Wang, K. Liu, J. Liu, Z. T. Yu, X. Xu, L. Zhao, T. Lee, E. K. Lee, J. Reiss, Y. K. Lee, L. W. Chung, J. Huang, M. Rettig, D. Seligson, K. N. Duraiswamy, C. K. Shen and H. R. Tseng, *Angew Chem Int Edit*, 2011, 50, 3084-3088.
4. H. Zhang, L. Liu, C. W. Li, H. Y. Fu, Y. Chen and M. S. Yang, *Biosens Bioelectron*, 2011, 29, 89-96.
5. W. Q. Yue, H. Zou, Q. H. Jin, C. W. Li, T. Xu, H. Y. Fu, L. C. H. Tzang, H. Y. Sun, J. L. Zhao and M. S. Yang, *Biosens Bioelectron*, 2014, 54, 297-305.
6. J. A. Davis, D. W. Inglis, K. J. Morton, D. A. Lawrence, L. R. Huang, S. Y. Chou, J. C. Sturm and R. H. Austin, *P Natl Acad Sci USA*, 2006, 103, 14779-14784.
7. H. Amini, E. Sollier, M. Masaeli, Y. Xie, B. Ganapathysubramanian, H. A. Stone and D. Di Carlo, *Nat commun*, 2013, 4, 1826.
8. C.-W. Li and M. Yang, *Lab Chip*, 2007, 7, 1712-1716.
9. R. F. Ismagilov, D. Rosmarin, P. J. A. Kenis, D. T. Chiu, W. Zhang, H. A. Stone and G. M. Whitesides, *Anal Chem*, 2001, 73, 4682-4687.
10. H. M. Xia, S. Y. Wan, C. Shu and Y. T. Chew, *Lab Chip*, 2005, 5, 748-755.
11. D. Lee and P. H. Lo, *Chem Eng J*, 2012, 181, 524-529.
12. H. Chen and J.-C. Meiners, *Appl Phys Lett*, 2004, 84, 2193.
13. M. Kuhn, M. Campillos, P. Gonzalez, L. J. Jensen and P. Bork, *FEBS lett*, 2008, 582, 1283-1290.
14. G. W. Mihaly, M. S. Ching, M. B. Klejn, J. Paull and R. A. Smallwood, *Brit J Clin Pharmaco*, 1987, 24, 769-774.
15. Y. Z. Zhang and H. Gorner, *Photochem Photobiol*, 2009, 85, 677-685.
16. D. Gao, Y. Tian, F. Liang, D. Jin, Y. Chen, H. Zhang and A. Yu, *J Lumin*, 2007, 127, 515-522.
17. N. J. Waters, R. Jones, G. Williams and B. Sohal, *J Pharm Sci*, 2008, 97, 4586-4595.
18. B. Huang, H. Wu, S. Kim and R. N. Zare, *Lab Chip*, 2005, 5, 1005-1007.
19. C.-W. Li, C. N. Cheung, J. Yang, C. H. Tzang and M. Yang, *Analyst*, 2003, 128, 1137.
20. C.-W. Li, R. Chen and M. Yang, *Lab Chip*, 2007, 7, 1371-1373.
21. W. Q. Yue, C. W. Li, T. Xu and M. S. Yang, *Lab Chip*, 2011, 11, 3352-3355.
22. Y. Luo, F. Yu and R. N. Zare, *Lab Chip*, 2008, 8, 694-700.
23. H. Wu, B. Huang and R. N. Zare, *Lab Chip*, 2005, 5, 1393-1398.
24. C. W. Li, J. Yang and M. S. Yang, *Lab Chip*, 2006, 6, 921-929.
25. K. P. Nichols, J. R. Ferullo and A. J. Baeumner, *Lab Chip*, 2006, 6, 242-246.
26. A. D. Stroock, S. K. W. Dertinger, A. Ajdari, I. Mezic, H. A. Stone and G. M. Whitesides, *Science*, 2002, 295, 647-651.
27. B. H. Weigl and P. Yager, *Science*, 1999, 283, 346-347.
28. N. Muramatsu and A. P. Minton, *P Natl Acad Sci USA*, 1988, 85, 2984-2988.
29. P. O. Gendron, F. Avaltroni and K. J. Wilkinson, *J Fluoresc*, 2008, 18, 1093-1101.
30. P. W. Atkins, *Physical Chemistry*, Oxford University Press, UK, 1994.
31. S. Yang, A. Undar and J. D. Zahn, *Lab Chip*, 2006, 6, 871-880.
32. T. O. Peulen and K. J. Wilkinson, *Environ Sci Technol*, 2011, 45, 3367-3373.
33. Y. N. Du, M. J. Hancock, J. K. He, J. L. Villa-Uribe, B. Wang, D. M. Cropek and A. Khademhosseini, *Biomaterials*, 2010, 31, 2686-2694.
34. M. Yang, C. W. Li and J. Yang, *Anal Chem*, 2002, 74, 3991-4001.
35. T. Xu, W. Q. Yue, C. W. Li, X. S. Yao, G. P. Cai and M. S. Yang, *Lab Chip*, 2010, 10, 2271-2278.

36. Y. Ni, Q. Liu and S. Kokot, *Spectrochim Acta A*, 2011, 78, 443-448.
37. A. A. Waheed and P. D. Gupta, *J Biochem Bioph Meth*, 2000, 42, 125-132.